Eletrônica de Potência
Open Journal of Power Electronics

Received July 27, 2024; accepted September 16, 2024; Date of publication October 02, 2024.
The review of this paper was arranged by Associate Editor Roberto F. Coelho and Editor-in-Chief Heverton A. Pereira.

Digital Object Identifier http://doi.org/10.18618/REP.e202436

Analog One-Cycle Control Strategy for Stable Battery Charging in Photovoltaic Systems

João T. de Carvalho Neto[1], **Andres O. Salazar**[2]

[1]Federal Institute of Education, Science and Technology of Rio Grande do Norte, Natal-East Side Campus, Natal - RN, Brazil.
[2]Federal University of Rio Grande do Norte, Departamento de Engenharia de Computação e Automação, Natal - RN, Brazil.

e-mail: joao.teixeira@ifrn.edu.br; andres@dca.ufrn.br.

ABSTRACT The growing adoption of photovoltaic systems for direct electricity generation from solar radiation has underscored the importance of efficient energy storage solutions. Batteries are the predominant method for storing energy from photovoltaic systems, especially for applications such as electric vehicle (EV) charging. However, these systems face significant challenges, particularly regarding battery longevity, as fluctuations in solar irradiation can lead to harmful voltage spikes. This paper introduces an Analog One-Cycle Control (OCC) strategy designed to mitigate these issues by stabilizing the battery voltage against varying input voltages. The proposed control scheme aims to enhance battery life by preventing damage caused by voltage overshoots. Experimental results demonstrate the effectiveness of the OCC strategy in maintaining steady-state conditions and optimizing power management.

KEYWORDS Battery Longevity, One-Cycle Control, Photovoltaic Systems, Voltage Stabilization.

I. INTRODUCTION

The use of photovoltaic (PV) energy is increasing significantly in various applications, with a particular focus on battery charging for electric vehicles. This increase is due to the growing demand for sustainable and clean energy sources and advances in solar power technology. PV systems use sunlight to generate electricity, making them an environmentally friendly alternative to fossil fuels.

Using solar power to charge electric vehicles (EVs) offers many benefits, including reduced greenhouse gas emissions, energy independence, and lower costs. By integrating PV modules into charging stations, EVs will be able to run on clean energy, minimizing their carbon footprint and contributing to the overall sustainability of transportation. This trend highlights a promising transition to a greener future, with PV playing a key role in powering EVs and promoting sustainable mobility solutions. The works in the literature highlights the increasing applications of gridable EVs (GEVs) and explores the opportunities and challenges associated with their integration into the power grid. GEVs, which encompass vehicle-to-home, vehicle-to-vehicle and vehicle-to-grid technologies, hold significant potential to transform our society [1].

One-cycle control (OCC) is a power electronics control method that aims to achieve accurate and efficient control of power converters. This technique is particularly relevant in battery charging situations where precise control and regulation of charge current and voltage is essential for optimal battery performance and life [2]. One of the main advantages of OCC is its ability to provide fast dynamic response and tight control. By using a single cycle of the input waveform, the control algorithm ensures that the converter's output quickly tracks and adjusts for the desired charging characteristics [3], [4]. This allows for efficient and reliable battery charging while minimizing overshoot and undershoot. In addition, OCC technique has inherent advantages in terms of simplicity and cost effectiveness in analog and digital implementations [5]. This simplicity not only reduces system complexity, but also increases reliability and reduces manufacturing costs. Additionally, the inherent robustness of the OCC technique makes it suitable for a wide variety of battery charging applications. It can accommodate different battery chemistries and operating conditions without compromising performance, adapting to changing loads and varying input voltages. OCC offers versatile applications in a variety of power electronic systems. Notable examples include motor control systems, power factor correction (PFC) [6], uninterruptible power supplies [7], active power filters [8] and grid-tied inverters [6], [9]. The use of OCC in these applications allows for precise and efficient control of the power conversion process, resulting in improved system performance, reduced energy loss, and increased overall system reliability.

Several works present charging batteries methods using PV energy, connecting a PV module directly to the battery without changing direct current to alternating current. Although this system is simple, there are some drawbacks to consider. Therefore, it is very important to insert the controller between the PV source and the battery during the charging process. This controller is a DC-DC converter, and its role needs to supply the battery with the maximum power generated by solar energy during the battery charging process, regardless of the climatic conditions and without causing disturbances in the battery.

Some techniques are capable of rejecting perturbation from the power source without causing disturbances in the battery. A disturbance observer-based model predictive voltage

control method to improve the power quality of electric vehicle charging stations with battery energy storage systems is proposed in [10]. A grid interface current control strategy for a DC microgrid, which aims to reduce the disturbance from PV generation and the load variation to the main grid without a grid interface converter, is presented in [11].

Some battery charging applications use MPPT (maximum power point tracking) methods that minimize the effects of overshoots caused by sudden changes in irradiance. The constant voltage (CV) method is a simple method, which has good efficiency in locations with few temperature variations and guarantees constant voltage in the photovoltaic modules even in sudden variations in irradiance, minimizing the effects of overshoots on the batteries, prolonging their useful lifetime [12].

The development and optimization of Battery Energy Storage Systems (BESS) for renewable energy applications have been extensively studied in recent years. One notable methodology is the Choice Matrix Approach, which assists in the design of BESS by evaluating multiple criteria such as system dc-link voltage, battery lifetime, and storage capacity index. This approach, as detailed by recent studies, employs Multiple Criteria Decision Making (MCDM) to balance Operational Expenditure (OPEX) and Capital Expenditure (CAPEX) considerations, providing a comprehensive framework for selecting the most suitable battery for specific applications like peak shaving in photovoltaic (PV) systems [13].

Furthermore, the dynamic modeling of BESS for ancillary services provision has been a crucial aspect of integrating these systems into power grids. Research has focused on adapting models to platforms for simulating electromechanical transients, enhancing the accuracy and reliability of BESS operation under various scenarios, including normal operation and external events. The comparison of these models with other established platforms demonstrates the effectiveness of these implementations in maintaining consistent performance and flexibility in BESS representation [14].

The work proposed in [15] presents a battery charging system using the One-Cycle Control (OCC) technique implemented in an analog manner with experimental results, demonstrating the functionality of the battery charging controller in both current and voltage modes. Building on this foundation, the present article offers new experimental results, including a more in-depth analysis of the ideal operating points in each charging mode and a comparison of these points with the experimental results obtained. Additionally, the test parameters were adjusted to better align the results with real-world conditions. This comprehensive evaluation provides further insights into the efficiency and robustness of the OCC technique in practical applications.

The proposed system in this work can be utilized in various energy storage applications, including BESS, electric vehicles, backup power supplies for critical infrastructure, and grid stabilization in microgrid environments. The system's power stage can be resized according to the specific power requirements of the application, ensuring adaptability for different use cases.

In order to take advantage of OCC and CV MPPT method, this work aims to present the experimental results of a control strategy applying OCC and Constant Voltage MPPT method and an OCC voltage regulator in battery charging using PV energy. Steady-state control and power signals are presented, validating the use of the technique in the proposed system.

II. SYSTEM PRESENTATION

A. *System Overall*

The system proposed in this study consists of a PV module, a DC-DC boost converter, a battery bank, and an OCC-based control system. The electrical schematic of the proposed system is shown in Fig. 1. The PV module is responsible for supplying power to the battery bank through a power stage controlled by the DC-DC boost converter. This converter calculates the power stage required based on the input from the PV module. The batteries can be charged in two modes: current mode and voltage mode. In current mode, the OCC-based MPPT Controller plays a crucial role by tracking the maximum power point of the PV module. It does this by continuously reading the input voltage from the PV module and calculating the appropriate duty cycle to control the switching of the DC-DC converter. This ensures that the PV module operates at its maximum power point, delivering optimal power to charge the battery bank. Once the maximum State-Of-Charge (SOC) is reached, the system automatically transitions to voltage mode implemented by the OCC Based Voltage Regulator Controller. In this mode, the OCC controller switches to regulating the voltage to maintain it at the floating voltage level, which is essential for preserving battery health. A low current is used in this mode to keep the batteries fully charged without overloading them. The system utilizes a multiplexer as a charging mode selector, which dynamically switches between the current mode and voltage mode duty cycles depending on the battery bank's charge state.

B. *Control Strategy*

The OCC is a non-linear control approach that, according to K. M. Smedley [16], achieves the average value of dynamic control of a switching variable in one clock cycle. The primary characteristic of the OCC modulation is that it

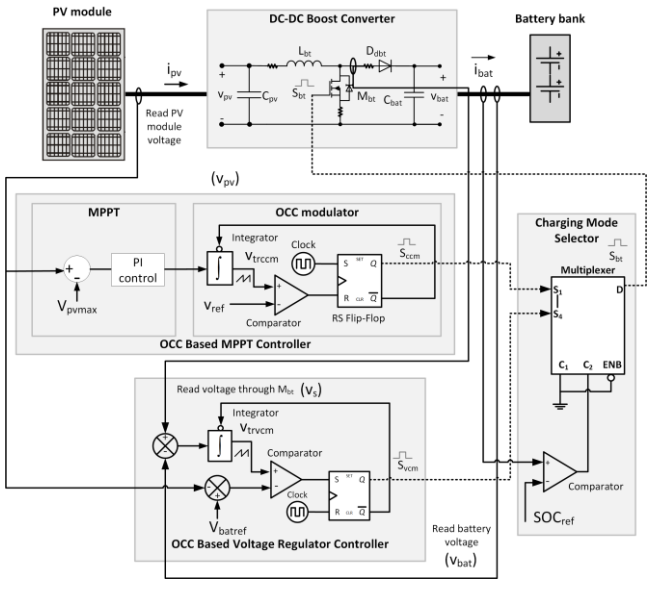

Figure 1. Electrical schematic of the proposed system.

controls a carrier's amplitude rather than the control variable, as is typically the case with other modulations like PWM (Pulse Width Modulation). In the method, a medium dynamic control a switching variable is reached after a system transition in just one clock cycle. Thus, the OCC is a nonlinear control approach that is appropriate for the nonlinear switching nature of switched converters. In OCC modulator (Fig. 1), the switching variable is integrated, and its value (V_{trccm}) increases until a reference value (v_{ref}) and then drops to zero. The switching variable starts to increase again in the next pulse of the clock. The results is a modulated width pulse responsible for switching the Mosfet M_{bt}.

In current mode, the OCC based MPPT controller uses the simple constant voltage (CV) scheme once it has several advantages over other iterative schemes such as P&O (Perturb and Observe) and Incremental Conductance (IC) when charging a battery. These two methods have the property of have oscillations in steady state conditions, which is undesirable for battery charging. The reason for adopting the CV method is that it has high reliability, little oscillation, and high tracking efficiency to the maximum power point. The main drawback of this method is that this maximum supply voltage can vary significantly with temperature [12]. Therefore, it can be used in an environment with little temperature change. The advantage of this method is that only one voltage sensor is required at the module output and maximum performance can be reached with a simple Proportional-Integrative control loop.

In voltage mode, the OCC based voltage regulator controller is responsible for making the battery fluctuating after the full SOC. The implementation of this controller is obtained through the Boost switching operation characteristics [16]. When the boost MOSFET (M_{bt}) is off (during T_{off}), the diode D_{dbt} becomes forward-biased, and the voltage across the diode is zero. When the MOSFET (M_{bt}) is on (during T_{on}), the diode D_{dbt} is reverse-biased and therefore non-conductive, and its voltage is equal to the difference between the input voltage (v_{pv}) and the output voltage (v_{bat}). Considering v_{sbt}, the voltage through the Mosfet, d_b the Boost duty-cycle, T_s the switching period, the equation of voltage mode controller can be shown in (1).

$$v_{pv} - V_{batref} = \frac{1}{T_S} \int_0^{d_b T_S} (v_{sbt} - v_{bat})\, dt \qquad (1)$$

Where: v_{pv} is the PV voltage, V_{batref} is the reference voltage when the battery reaches its full SOC, v_{sbt} is the voltage at the converter Mosfet, v_{bat} is the battery voltage, T_s is the switching period and d_b is Boost duty-cycle. A Charging Mode Selector implemented with a multiplexer is responsible to change the battery charging mode from current mode to voltage mode when the full SOC is reached.

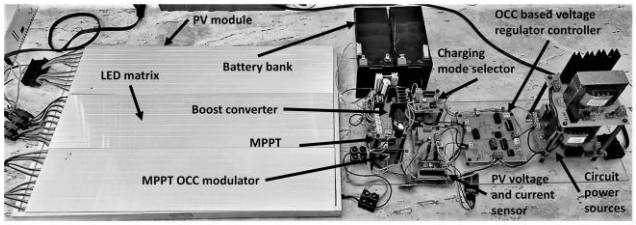

Figure 2. Laboratory experimental system.

III. EXPERIMENTAL RESULTS

A. *Experimental Parameters*

The experimental system is presented in Fig. 2. The system's PV source is a Yingli-20 PV model with the specifications under Standard Test Conditions (STC), irradiance of 1000 W/m², temperature of 25 °C and Air Mass Index (AM) 1.5: Maximum Power Voltage (V_{pvmax}) of 16.9 V, Maximum Current (I_{pvmax}) of 1.17A, Maximum Power (P_{pv}) of 20W. The system's battery bank is composed of two 12 V batteries connected in series, with the following specifications for each: floating voltage (V_{batref}) of 13.2 V, maximum current of 1.35 A. The experimental tests were conducted with the photovoltaic module operating at a temperature of 35°C. Table I presents the main experimental system specifications.

TABLE 1. Experimental System Specifications.

Variable	Value	Description
C_{pv}	680 uF	PV parallel capacitor
L_{bt}	2.85 mH	Boost inductor
C_{bat}	680 uF	Boost output capacitor
V_{pvmax}	16.3 V	Maximum Power Voltage at 1000W/m² and 35°C
V_{batref}	26.4 V	Voltage reference at voltage mode
v_{ref}	16.3 V	PV voltage reference at current mode
SOC_{ref}	26.4 V	Reference for battery control toggle
K_p	5	PI control proportional constant
T_i	0.001 s	PI control integration time
T_s	0.00005 s	Clock switching time period

Figure 3 presents the characteristic curves of the Yingli-20 PV module under different irradiances at this operating temperature. Figure 3 includes a 16.3 V line, with intersection points representing the operating points corresponding to battery charging in current mode. Figure 3 was generated through a simulation of the PV module using the Powersim PSIM software. Table 2 presents the maximum power (P_{pv}), current at maximum power (I_{pv}) and open circuit voltage (V_{oc}) of the photovoltaic module obtained through simulation, considering the irradiances and temperatures adopted in the experimental results.

TABLE 2. Electrical variables of the PV module obtained through simulation, considering the irradiances and PV module temperature at 35°C adopted in the experimental results.

Irradiance (W/m²)	P_{pv} (W)	I_{pv} (mA)	V_{oc} (V)
1000	19.14	1174	19.48
900	17.11	1050	19.35
800	15.08	924	19.23
700	13.05	799	19.07
600	11.01	674	18.90
500	8.98	550	18.69
400	6.95	425	18.43
300	4.92	300	18.10
200	2.89	176	17.66
100	0.85	51	16.88

The battery bank is composed of two sealed lead-acid batteries in series with the following recommended parameters operating at 25 ºC: floating voltage of 13.5 V to 13.8 V, cyclic voltage of 14.4 V to 14.9 V, cut-off voltage of 10.5 V and maximum current of 1.35 A. The accepted minimum floating voltage for this kind of battery is 13.1 V.

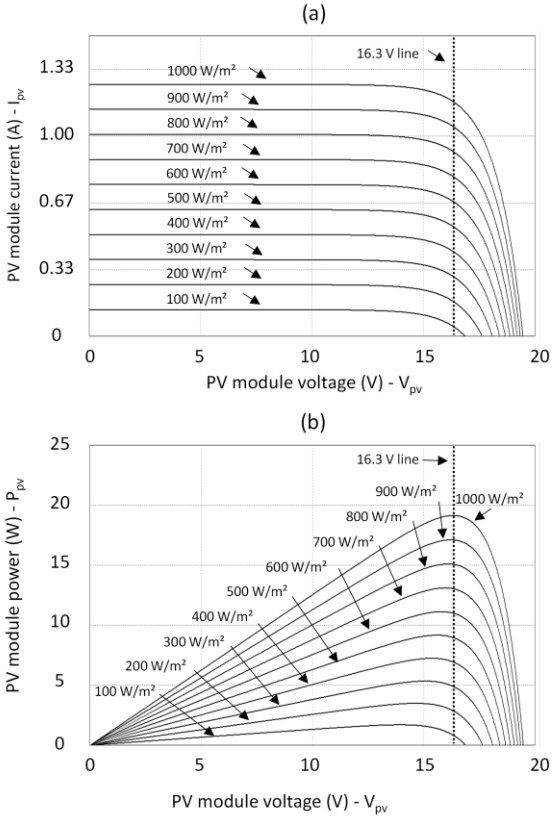

Figure 3. Yingli-20 PV module characteristic curves at 35°C considering different irradiance conditions: (a) I_{pv} x V_{pv} (b) P_{pv} x V_{pv}.

Figure 4 illustrates the system's operating points at current mode, establishing the Boost converter's output voltage (battery charging voltage) as a function of its duty cycle. It is important to note that the input voltage to the Boost converter is fixed at 16.3 V through the constant voltage MPPT. The graph in Figure 4 represents the minimum voltage of both batteries in series at the cyclic voltage (28.8V) and the maximum cyclic voltage, which can exceed 14.9 V for each battery, taking into account that the temperature during the experimental test ranges from 18°C to 23°C.

Figure 5 presents the operating points in the constant voltage charging mode. The graph was obtained using the Boost converter equation, considering a constant output voltage for the batteries (V_{batref}) of 26.4 V. In this mode of operation, the PV module operates at voltages close to the PV open-circuit voltages, where the current from the PV source is nearly zero, keeping the batteries charged under low current. The operation curve shown in the graph spans the range between the open-circuit voltage corresponding to 100 W/m² of approximately 16.88 V and that corresponding to 1000 W/m² of approximately 19.48 V, as obtained from Table 2.

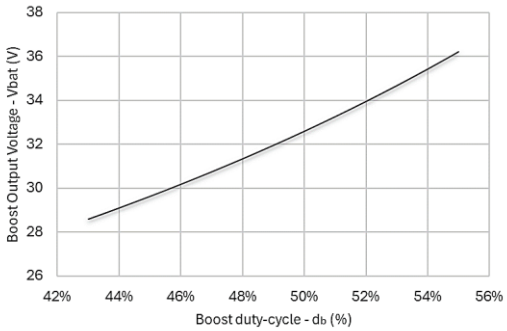

Figure 4 – Boost converter operating curve at current mode, considering v_{pv} of 16.3 V.

Considering the battery bank is implemented with two batteries in series, and the minimum floating voltage is 13.1 V, the reference voltage (V_{batref}) and the full State of Charge reference (SOC_{ref}) were adjusted to a slightly higher value of 26.4 V (13.2 v per battery). Voltage sensors are implemented by a voltage divisor with constant of 6. The current values from the current sensors are obtained through the equations in Fig. 6 and Fig. 7.

The current sensor for the photovoltaic module (I_{pv}) is a Hall effect sensor, the HCS-LSP 06A, with a maximum current reading capacity of 6 A. In this sensor, the current reading generates an offset voltage of 2.37 V, and the maximum current of 6 A corresponds to an output voltage of 2 V, linearly. To improve the resolution of current-to-voltage conversion, the sensor's windings were designed to provide a gain of 0.578 relative to the sensor's output voltage. Thus, equation (2) represents the measured I_{pv} current as a function of the output voltage from the Hall sensor.

$$I_{pv} = 0.578 \cdot (\text{measured voltage} - 2.37) \quad (2)$$

The current sensor for the battery bank current (I_{bat}) is another Hall effect sensor, the TBC03SYH, with a maximum current reading capacity of 3 A. This sensor has an internal winding where the 3 A current is represented by an output voltage of 4 V in a linear relationship. This is reflected in equation (3).

$$I_{bat} = 0.75 \cdot \text{measured voltage} \quad (3)$$

The equation that implements the signal V_{trvcm} voltage was derived from a voltage divider in the controller with a multiplier of 4.5, as presented in equation (4).

$$V_{trvcm} = 0.45 \cdot \text{measured voltage} \quad (4)$$

B. *Test 1: Current Mode Test at Different Irradiances*

The tests in current mode were performed in laboratory considering the following irradiance conditions at 35 ºC: 100 W/m², 200 W/m², 300 W/m², 400 W/m², 500 W/m², 600 W/m² and 700 W/m². Due to electrical limitations, the maximum irradiance value obtained through the LED matrix

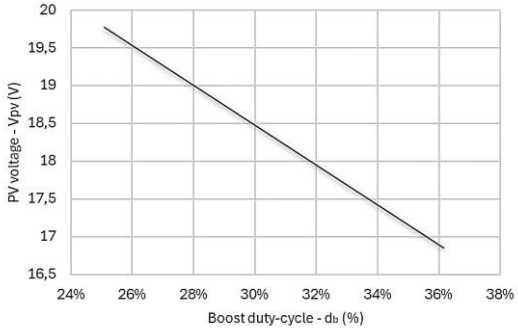

Figure 5 - Boost converter operating curve at voltage mode considering v_{bat} of 26.4V

was 700 W/m². The current mode test validated in this section present a steady state analysis of the voltages and currents of the photovoltaic module and the battery bank with the objective of validating the MPPT controller based on the constant voltage method and its robustness in different irradiance situations. The irradiance is controlled by an LED matrix installed on the surface of the PV module. Power signals in current mode obtained in oscilloscope are presented in Fig. 6 and Fig. 7.

The results presented in this work consider the maximum power relative to the module voltage of 16.3V, related to the maximum voltage of 1000 W/m² and 35 °C. In this way, v_{ref} was set to the reference value of 16.3 V. Table 3 presents the steady-state power variables and the Boost converter efficiency (η) in the mentioned conditions during current mode when the battery is discharged.

As consequence of CV mode MPPT, the voltage has practically the same value for all irradiance cases, having a small variation between 16.18 V and 16.4 V which corresponds to an error of 0.7 % and 0.6 %, respectively. The use of this MPPT together with the advantages inherent to the OCC already observed in this paper, guarantee the minimum of disturbance in the battery bank in sudden changes of irradiance.

As can be observed, as the irradiance increases, both the current provided by the PV module and the charging current of the batteries increase proportionally. This demonstrates the system's ability to effectively harness solar energy and convert it into electrical energy for battery charging.

TABLE 3. System Variables in Steady considering different irradiance conditions and 35 °C.

Variable	Irradiance (W/m²)						
	100	***200***	***300***	***400***	***500***	***600***	***700***
V_{pv} (V)	16.2	16.18	16.4	16.32	16.25	16.4	16.2
I_{pv} (mA)	63	201	294	433	530	663	756
V_{bat} (V)	26.80	30.40	31.60	32.00	32.43	33.20	32.80
I_{bat} (mA)	7	49	104	166	222	273	341
P_{pv} (W)	1.03	3.25	4.82	7.06	8.61	10.88	12.24
P_{bat} (W)	0.18	1.49	3.28	5.33	7.22	9.06	11.18
η (%)	18	46	68	75	84	83	91

It is evident that higher irradiance levels result in higher battery charging voltages. This can be attributed to the increase in battery charging current, which is more significant at higher irradiances. For instance, at an irradiance of 100 W/m², the PV module provides a voltage of 16.2 V and a current of 63 mA, resulting in a power output of 1.03 W. The corresponding battery voltage is 26.80 V with a charging current of 7 mA, leading to a power injection of 0.18 W into the battery. The efficiency of the boost converter at this irradiance is 18%. The low charging current at this level justifies the battery charging voltage being lower than 14.4 V

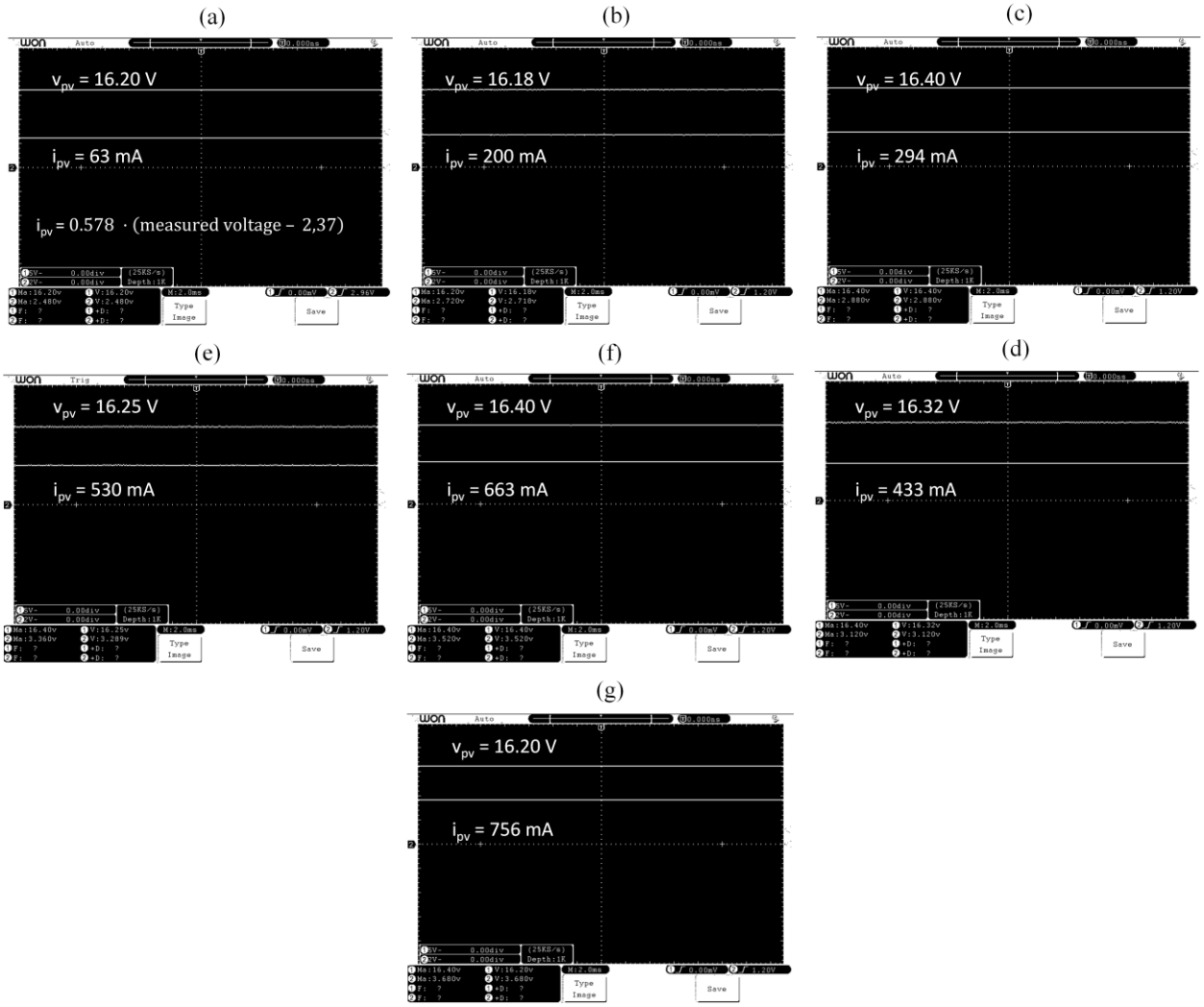

Figure 6. PV current and voltage considering PV temperature of 35 °C and different irradiance conditions: (a) 100 W/m²; (b) 200 W/m²; (c) 300 W/m²; (d) 400 W/m²; (e) 500 W/m²; (f) 600 W/m²; (g) 700 W/m².

per battery, i.e., below 28.8 V for the series configuration, which explains the low efficiency of the system under this condition.

As the irradiance increases to 700 W/m², the PV module voltage remains relatively stable around 16.2 V, while the current rises significantly to 756 mA, yielding a power output of 12.24 W. The battery voltage at this level is 32.80 V with a charging current of 341 mA, resulting in a power injection of 11.18 W. The efficiency of the boost converter improves to 91% at this irradiance level, indicating the system's enhanced performance under higher solar irradiance.

These results highlight that the system exhibits higher efficiency at higher irradiances, showing that the charging process is more effective as the irradiance increases. The minimum charging voltage for the batteries is achieved at irradiances of 200 W/m² and above, where the charging voltage reaches the necessary level of 28.8 V for the series configuration. This underscores the importance of sufficient irradiance for optimal system efficiency.

C. *Test 2: Current and Voltage Modes Signal Analysis*

In this section, the control signals are analyzed in both modes (current and voltage). In current mode the PV module operates at 16.2 V and the batteries voltage is 29.4 V. In voltage mode the PV module operates close to open circuit voltage point at 18.6 V while the batteries voltage is 26.4 V (floating voltage). Figures 8 and 9, shows the control signals (OCC carrier and the Pulse Width Modulated waves) in steady state during current mode and voltage mode, respectively.

During the tests performed to obtain Fig. 8, v_{pv} is 16.2 V and v_{bat} is 29.4 V which corresponds to the approximate obtained value of the duty cycle (d_b) (48.7 %). It is important to consider that the width of the generated PWM signal is proportional to the width of the sawtooth signal. However, due to the delay generated by the OCC analog integrator reset, there is a small error between the duty cycle of the sawtooth signal (41.7%) and the DC-DC converter switching signal (48.7%). This error is generated by the discharge time of the OCC controller integrator capacitor.

Ideally, the expected duty cycle the Boost converter equation would be 44.2%, showing a deviation of 9.3% in relation to the obtained duty-cycle of 48.7%. When comparing these values with the expected results from Figure 4, it is observed that the point on the curve corresponding to a v_{bat} of 29.4 V aligns with a duty cycle of approximately 45%. The error in the observed duty cycle is 3.7% (48.7% - 45%), which can be attributed to several factors. First, the curve in Figure 4 was developed for a PV module voltage of

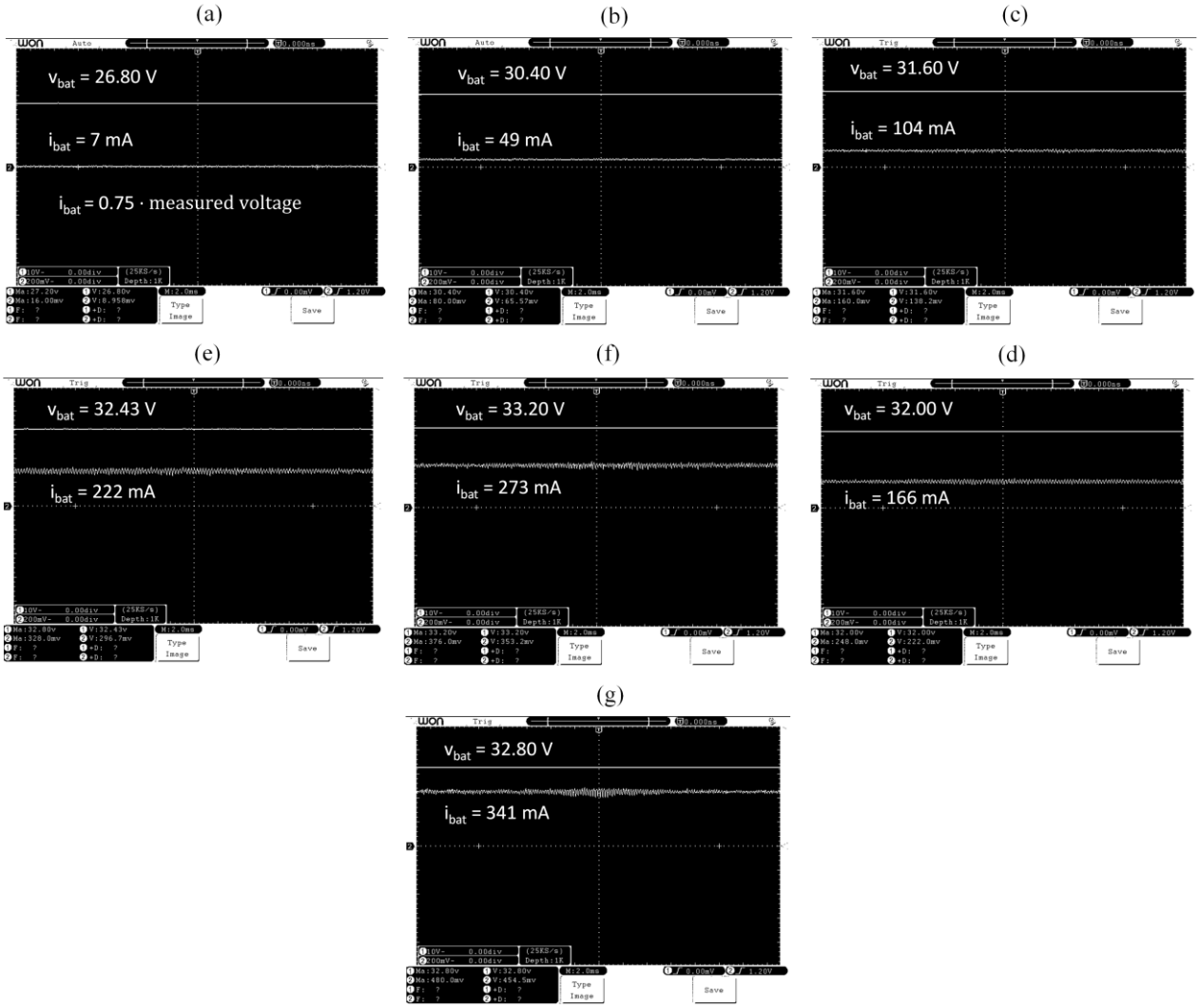

Figure 7 - Battery bank current and voltage considering PV temperature of 35 °C and different irradiance conditions: (a) 100 W/m²; (b) 200 W/m²; (c) 300 W/m²; (d) 400 W/m²; (e) 500 W/m²; (f) 600 W/m²; (g) 700 W/m².

16.3 V, whereas the experimental test used a PV module voltage of 16.2 V. This slight difference in input voltage affects the duty cycle, as the converter must adjust to maintain the desired output voltage. Additionally, real-world factors such as converter losses, including resistive losses in components, switching losses, and inductor core losses, contribute to the discrepancy. These losses are not accounted for in the ideal Boost converter equation but have some impact on the actual performance. However, as observed, a 3.7% error is considered quite small, emphasizing the robustness of the controller. This small deviation indicates that the controller is effectively managing the variations and losses inherent in practical applications, maintaining a high level of performance and reliability.

In voltage mode, the PV module stops operating at MPP and starts operating at v_{pv} voltage of 18.6 V and the v_{bat} is 26.40 V, which corresponds to the approximate obtained value of the duty cycle (d_b) (31.7 %). Notice that the switching duty-cycle is equal to the period of the integration of the switching variable. According to (1), the maximum amplitude of V_{trvcm} is equal to the difference between v_{pv} and V_{batref}. The maximum value of V_{trvcm} obtained is 9 V and the real value is 7.8 V which corresponds to an error of 13 %.

According to Figure 5, for an output voltage (v_{bat}) of 26.4 V, the ideal graph shows the relationship between Vpv and the duty cycle of around 29.5%. This is very close to the experimentally obtained duty cycle of 31.7%, indicating a minimal error of 6.8 %. This slight discrepancy can be attributed to practical factors such as converter losses, component tolerances, and the dynamic response of the control system. The comparison demonstrates that the experimental results closely match the expected values derived from the ideal graph. The small error of 6.8% highlights the robustness and accuracy of the controller in maintaining the desired output voltage under varying conditions.

The correlation between the experimental and ideal values validates the system's design and confirms its capability to operate within expected parameters, ensuring optimal performance in practical applications.

IV. CONCLUSIONS

This paper presents a photovoltaic system designed to charge a battery bank using an analogically implemented One-Cycle Control method. The system operates in two modes: current control and voltage control. In current control mode, the controller optimizes charging time by delivering maximum power to the battery through the Constant Voltage (CV)

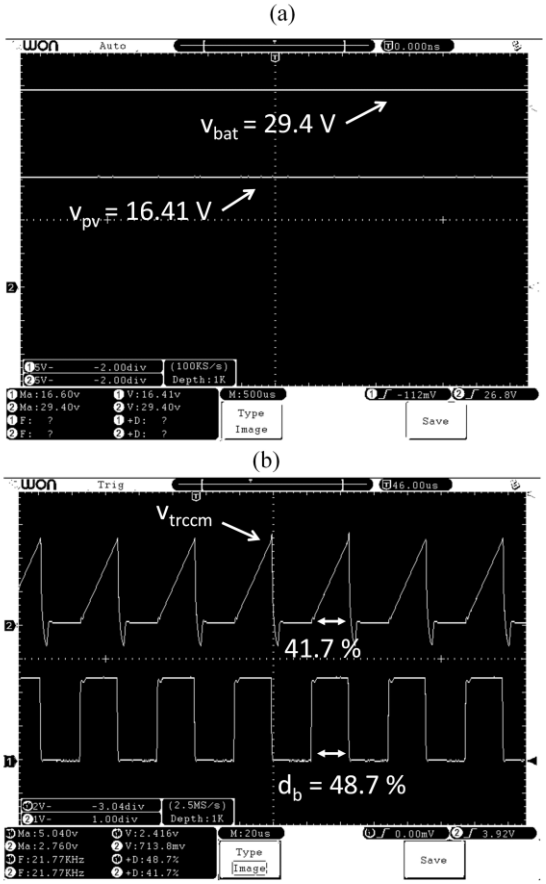

Figure 8. Control signals at steady-state conditions in voltage mode: (a) PV voltage (v_{pv}) and Batteries voltage (v_{bat}), (b) Duty Cycle of Modulated Signal (D_b) and triangular carrier (V_{trvcm}).

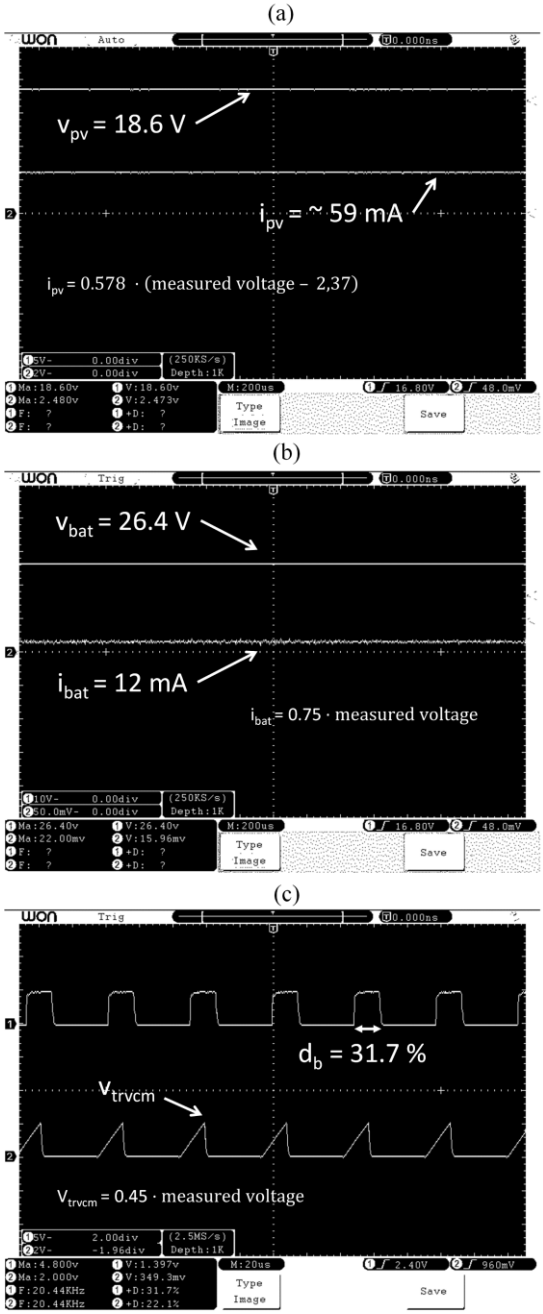

Figure 9. Control signals at steady-state conditions in current mode: (a) PV voltage (v_{pv}) and Batteries voltage (v_{bat}), (b) Duty Cycle of Modulated Signal (D_b) and triangular carrier (V_{trccm}).

Maximum Power Point Tracking (MPPT) method. In voltage control mode, the OCC regulates the battery at its floating voltage. A multiplexer switches from current mode to voltage mode when the battery bank is fully charged.

Experimental results demonstrate that in current mode, the system effectively manages irradiance fluctuations, consistently delivering a stable voltage according to its capacity. The robustness of the OCC technique in battery charging applications is highlighted by its ability to generate the PWM signal duty cycle from the width of the sawtooth signal, modulated by a switching variable at each clock cycle. In control signal analysis, the observed error between the expected duty cycle and experimental results, approximately 3.7% and 6.8% for current and voltage modes respectively, is mainly due to DC-DC converter losses and delays caused by the reset of the OCC integrator. These issues could be mitigated by implementing a digital OCC controller. Despite these minor drawbacks, the analog OCC controller offers a simple and cost-effective solution.

The results validate the application of OCC for charging batteries in both current and voltage modes. The use of OCC modulators significantly enhances performance, as OCC is known to minimize voltage overshoot and undershoot in battery applications. The advantages of the CV MPPT method in maintaining a steady-state constant voltage for the PV module, combined with the fast, accurate, and robust control capabilities of the OCC technique, make it an excellent choice for optimizing battery charging efficiency. This approach not only extends battery life but also ensures reliable operation.

In conclusion, the findings confirm the effectiveness of the OCC method for battery charging in PV systems, demonstrating its potential for practical applications in renewable energy systems.

ACKNOWLEDGMENT

The authors thank the Federal Institute of Education, Science, and Technology of Rio Grande do Norte for the support and encouragement in fostering research and enabling the publication of this work.

AUTHOR CONTRIBUTION

DE CARVALHO NETO, J.T. and **SALAZAR, A.O.**: Conceptualization, Data Curation, Formal Analysis, Funding Acquisition, Investigation, Methodology, Project Administration, Resources, Software, Supervision, Validation, Visualization, Writing – Original Draft, Writing – Review & Editing.

PLAGIARISM POLICY

This article was submitted to the similarity system providedby Crossref and powered by iThenticate – Similarity Check.

REFERENCES

[1] C. Liu, K. T. Chau, D. Wu, and S. Gao, “Opportunities and challenges of vehicle-to-home, vehicle-to-vehicle, and vehicle-to-grid technologies,” *Proceedings of the IEEE*, vol. 101, no. 11, pp. 2409–2427, 2013, doi: 10.1109/JPROC.2013.2271951.

[2] F. Yang, Y. Liu, W. Liu, and K. Yao, “One-Cycle Control for Pulse Power Generator in Electrical-Discharge-Machining,” *IEEE Transactions on Industrial Electronics*, vol. 69, no. 11, pp. 11012–11022, Nov. 2022, doi: 10.1109/TIE.2021.3121706.

[3] M. Shahabi, A. A. Koosha, and K. Abbaszadeh, "The Assessment of PI and Optimized OCC Control Methods in Buck Converter," in *2020 11th Power Electronics, Drive Systems, and Technologies Conference (PEDSTC)*, 2020. doi: 10.1109/PEDSTC49159.2020.9088395.

[4] Y. L. Guo, Q. H. Wu, L. Wang, and G. F. Tang, “Stability Enhancement of One-Cycle Controlled Buck-Boost Converters with a Composite Function Embedded,” *IEEE Transactions on Circuits and Systems I: Regular Papers*, vol. 67, no. 10, pp. 3512–3520, Oct. 2020, doi: 10.1109/TCSI.2020.2993409.

[5] J. Yao, P. Jiang, T. Lin, and A. Abramovitz, “Extension of OCC Controller for High-Voltage-Gain PFC Applications,” *IEEE Transactions on Circuits and Systems II: Express Briefs*, vol. 70, no. 9, pp. 3449–3453, Sep. 2023, doi: 10.1109/TCSII.2023.3264771.

[6] A. Alves, M. Bento, and R. P. Santiago, “Hybrid One-Cycle Control Strategy for Buck+Boost PFC Battery Charger; Hybrid One-Cycle Control Strategy for Buck+Boost PFC Battery Charger,” 2019.

[7] N. F. A. Abdul Rahman and M. C. H. Che Abang, “One-Cycle Controller for UPS’s Buck Converter Operation,” in *ICPEA 2021 - 2021 IEEE International Conference in Power Engineering Application*, Institute of Electrical and Electronics Engineers Inc., Mar. 2021, pp. 1–5. doi: 10.1109/ICPEA51500.2021.9417755.

[8] L. Wang, X. Han, C. Ren, Y. Yang, and P. Wang, “A Modified One-Cycle-Control-Based Active Power Filter for Harmonic Compensation,” *IEEE Transactions on Industrial Electronics*, vol. 65, no. 1, pp. 738–748, Jan. 2018, doi: 10.1109/TIE.2017.2682021.

[9] N. Vamanan and V. John, “Dual-Comparison One-Cycle Control for Single-Phase Bidirectional Power Converters,” *IEEE Trans Ind Appl*, vol. 54, no. 5, pp. 4621–4631, Sep. 2018, doi: 10.1109/TIA.2018.2836359.

[10] D. J. Kim, B. Kim, C. Yoon, N. D. Nguyen, and Y. Il Lee, “Disturbance Observer-Based Model Predictive Voltage Control for Electric-Vehicle Charging Station in Distribution Networks,” *IEEE Trans Smart Grid*, vol. 14, no. 1, pp. 545–558, Jan. 2023, doi: 10.1109/TSG.2022.3187120.

[11] M. Alshareef, Z. Lin, F. Li, and F. Wang, “A Grid Interface Current Control Strategy for DC Microgrids,” *CES Transactions on Electrical Machines and Systems*, vol. 5, no. 3, pp. 249–256, Sep. 2021, doi: 10.30941/CESTEMS.2021.00028.

[12] S. R. Osman, N. A. Rahim, and J. Selvaraj, "Microcontroller Based Solar Battery Charging System with MPPT Features at Low Irradiance Condition," in *2013 IEEE Conference on Clean Energy and Technology (CEAT) 18-20 Nov. 2013, Bayview Hotel, Langkawi, Malaysia*, 2013, pp. 437-441. doi: 10.1109/CEAT.2013.6775671.

[13] R. C. De Barros, W. C. S. Amorim, W. do C. Boaventura, A. F. Cupertino, V. F. Mendes, and H. A. Pereira, “Methodology for BESS Design Assisted by Choice Matrix Approach,” *Eletrônica de Potência*, vol. 29, pp. 1-10, Jun. 2024, doi: 10.18618/rep.2005.1.019027.

[14] P. F. Torres *et al.*, “Modelo Dinâmico de Sistemas de Armazenamento de Energia em Baterias para Provimento de Serviços Ancilares,” *Eletrônica de Potência*, vol. 28, no. 2, pp. 94–106, May 2023, doi: 10.18618/rep.2023.2.0036.

[15] J. T. De Carvalho Neto and A. O. Salazar, “Analog One-Cycle Control Based Scheme for Battery Charging in Photovoltaic Systems,” in *COBEP 2023 - 17th Brazilian Power Electronics Conference and SPEC 2023 - 8th IEEE Southern Power Electronics Conference, Proceedings*, Institute of Electrical and Electronics Engineers Inc., 2023. doi: 10.1109/SPEC56436.2023.10408628.

[16] K. M. Smedley and S. Cuk, "One-Cycle Control of Switching Converters," *IEEE Transactions on Power Electronics*, vol. 10, no. 6, pp. 625-633, Nov. 1995. doi: 10.1109/63.471281.

BIOGRAPHIES

Joao T. de Carvalho Neto received the B.S., M.S., and Ph.D. degrees in computing engineering from the Federal University of Rio Grande do Norte, Natal, Rio Grande do Norte, Brazil, in 2010, 2012, and 2016, respectively. Since 2013, he has been a Professor with the Federal Institute of Education Science and Technology of Rio Grande do Norte (IFRN), Natal. His research interests include efficiency analysis of photovoltaic cells, autonomous and grid-connected photovoltaic systems, power converter design, maximum power point tracking, battery charging, electric vehicles, and linear and nonlinear controllers.

Andrés O. Salazar received his bachelor's degree in electrical engineering in 1981 from the National University of Engineering (UNI), Peru. He received his master's degree in electrical engineering in 1989 and his Ph.D. degree in 1994, both from the Federal University of Rio de Janeiro (UFRJ), Brazil. He obtained his Ph.D. from the University of Tokyo, Japan. Currently, he has been a professor at the Federal University of Rio Grande do Norte since 1994. His research focuses on the control of electric machines and power converters.